J. Chem. Sci. (2020) 132:26
https://doi.org/10.1007/s12039-019-1727-1

REGULAR ARTICLE

Preparation of Ni_2P on twinned $Zn_{0.5}Cd_{0.5}S$ nanocrystals for high-efficient photocatalytic hydrogen production

XIAOPENG ZHOU, LINXIN YIN, KAIQING DAI, XIANGYANG GAO, YANAN FENG, YAFEI ZHAO* and BING ZHANG
School of Chemical Engineering, Zhengzhou University, Zhengzhou 450001, People's Republic of China
E-mail: zhaoyafei007@126.com

MS received 16 July 2019; revised 17 September 2019; accepted 23 September 2019

Abstract. Developing efficient non-precious metal semiconductor photocatalysts is highly desirable for photocatalytically splitting water. In this work, the composite of the nanocrystal twinned $Zn_{0.5}Cd_{0.5}S$ (ZCS) solid solution decorated with highly dispersed Ni_2P nanoparticles was successfully formed by *in situ* growth method, and it exhibited remarkable photocatalytic hydrogen production activity of visible light. A high rate of hydrogen production of 30473 μmol h^{-1} g^{-1} was achieved, and the apparent quantum yield (AQY) was as high as 83.5% at 420 nm. Moreover, the sample could maintain outstanding photocatalytic hydrogenation activity after 4-cycle continuous catalytic process. The unique nano-twinned structure of ZCS and synergistic effects between the Ni_2P and the twinned ZCS are responsible for the dramatically improved catalytic activities of photocatalysts composite.

Keywords. photocatalysts; Ni_2P-$Zn_{0.5}Cd_{0.5}S$; hydrogen production; water splitting.

1. Introduction

Hydrogen energy has been widely recognized as an effective substitute to fossil fuels for its cleanliness and high-energy density.[1] Photocatalytic hydrogen evolution, which uses solar power to produce hydrogen efficiently, is a promising hydrogen production strategy.[2] Since the discovery of photocatalytic splitting water for hydrogen production with TiO_2, the development of new semiconductor catalysts presented an accelerating trend.[3] As is well known, photocatalytic activity is determined by the efficiency of transport and separation of electrons and holes generated by light, which greatly depends on the band energy levels and the microcrystal structure of the catalysts.[4] Therefore, it is highly desirable to refine the microstructure and reduce the band gap energy of semiconductor photocatalysts, which is advantageous for not only the separation of photoelectrons and holes, but also for the transport of holes.[5]

In the past decades, various semiconductors were discovered, such as oxides, metal sulfides and oxynitrides,[6–9] which have been identified as valid catalysts for photocatalytic hydrogen production.[10] Among them, cadmium sulfide (CdS) has gained extensive attention because of its relatively narrow band gap of 2.42 eV, which is more easily responsive for visible-light and more negative than the redox potential of H^+/H_2.[11] However, the practical application of CdS is limited due to its low apparent quantum yield resulting from rapid electron recombination and severe photocorrosion. To solve these problems, the construction of ternary metal sulfides provides a feasible strategy.[4,12,13] Ternary $Zn_xCd_{1-x}S$ is one of the widely used photocatalysts, because the band gap of $Zn_xCd_{1-x}S$ can be controlled and its conduction band can be shifted to a more negative position to improve the photocatalytic H_2 production activity. Even so, the single nanocrystal structure of $Zn_xCd_{1-x}S$ does not have a high enough efficiency for space charge separation, which greatly shortens the life of photo-generated carriers. Recently, some works reveal that the $Zn_xCd_{1-x}S$ with nano-twinned structure can improve the charge transport properties (due to its highly ordered structures) and offer effective spatial isolation

*For correspondence

Electronic supplementary material: The online version of this article (https://doi.org/10.1007/s12039-019-1727-1) contains supplementary material, which is available to authorized users.

Published online: 22 January 2020

of photo-generated electrons/holes to prevent their recombination (due to the possibility of forming electrostatic field).[5] This twinning structure is formed by alternating arrangements of zinc blende/wurtzite (ZB/WZ) and arranging the twinning superlattice periodically. The homojunctions between two different phases within the same nanocrystals can improve the separation efficiency of electron-hole pairs and reduce their recombination.[14,15] Supporting suitable cocatalysts onto semiconductors has been proved an effective method for further improving photocatalytic activity.[16] The cocatalyst can trap photogenerated charge, restrain the rapid recombination of electron/hole pairs and decrease the activation energy or overpotential of H_2 decomposition. At present, most reported cocatalysts are noble metals (such as Au and Pt),[17,18] however, the high price of precious metals makes their applications in hydrogen production impractical. Consequently, it is very crucial to develop the non-precious metal catalysts with cost-effective.[19] With the efforts of many groups, various promising cocatalysts including transition metal sulfides (Cu_2S, $Cu_{1.94}S$, NiS, Mo_2S and CoS),[20–24] hydroxides $Ni(OH)_2$, $Co(OH)_2$)[25,26] and transition metal phosphides (Cu_3P, Co_2P, CoP and Ni_2P)[27–30] have been developed. Among them, Ni_2P has particular optoelectronic properties and has been reported as a highly efficient and earth-abundant cocatalyst,[31] which significantly improves the activity of photocatalytic hydrogen production. Taking into account the characteristics of $Zn_xCd_{1-x}S$ and Ni_2P, it will be significant to couple N_2P with twinned $Zn_xCd_{1-x}S$, which can fully exploit the advantages of Ni_2P and $Zn_xCd_{1-x}S$. We expected that excellent photocatalytic performance can be achieved.

Herein, we develop a facile approach to grow Ni_2P on pre-synthesized twinned $Zn_{0.5}Cd_{0.5}S$ (ZCS) nanocrystals coupled with hydrothermal synthesis. To our knowledge, there is seldom research on photocatalytic performance of combining Ni_2P with twinned ZCS.[4] The as-prepared photocatalyst (Ni_2P-ZCS) exhibited excellent visible-light photocatalytic activity for hydrogen evolution with a high hydrogen production rate of 30473 μmol h^{-1} g^{-1}. The apparent quantum yield (AQY) could reach as high as 83.5% under visible light ($\lambda \geq 420$ nm), and the activity retention rate could maintain 90.5% of primitive H_2-evolution rate after 4-cycle continuous catalytic process for 16 h. Twinned ZCS offers high electron-hole pairs separation rate to a large extent, and Ni_2P not only restrains the rapid recombination of electron-hole pairs but also decreases the activation energy. Meanwhile, the synergistic effect between Ni_2P and ZCS can dramatically elevate the photocatalytic performance as well. The results reveal great potential of Ni_2P-ZCS as high-performance photocatalytic materials. Besides, the simple and scalable method employed in this work may be feasible for preparing other transition metal oxides (hydroxides)-ZCS-based composites with excellent photocatalytic performance, extending their potential applications in many fields.

2. Experimental

2.1 *Synthesis of twinned ZCS*

The twinned ZCS was formed by a hydrothermal precipitation method (Figure 1).[5] A certain amount of cadmium acetate (0.01 mmol) and zinc acetate (0.01 mmol) were added to the deionized water (40 mL), and then 10 mL of sodium hydroxide was added after mixing well. Next, 0.25 mmol of thioacetamide were added into suspension by stirring for 30 min and then transferred into a 100 mL Teflon-lined stainless-steel autoclave and maintained at 180 °C for 24 h. Twinned ZCS was obtained by rinsing the above solid with anhydrous ethanol and deionized water for three times, followed by vacuum drying at 60 °C for 12 h.

2.2 *Synthesis of Ni_2P-ZCS*

Ni_2P-ZCS composites were prepared by an *in situ* growth method (Figure 1).[32] 0.4 g of the as-prepared twinned ZCS was dissolved in ethylenediamine (60 mL), and then after stirring uniformly, a certain amount of $Ni(NO_3)_2{\cdot}6H_2O$ and excess red phosphorus nanoparticles (molar ratio of Ni to P is 1:5) were added to ensure completely phosphating. After continuous socinate for half an hour, the mixed homogeneous solution was transferred to 100 mL Teflon-lined autoclave and maintained at 160 °C for 24 h. Subsequently, the product was collected and washed with deionized water and anhydrous ethanol for three times. Finally, the product was dried in a vacuum oven at 80 °C for 5 h to obtain Ni_2P-

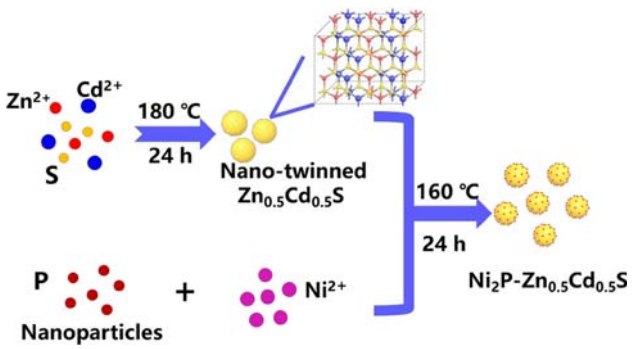

Figure 1. Schematic diagram of the synthesis procedures of Ni_2P-ZCS composite photocatalysts.

ZCS. For comparison, pure Ni_2P was also synthesized using the same method without adding of ZCS.

2.3 *Characterization*

X-ray diffraction (XRD) patterns of the prepared photocatalysts were confirmed by an X-ray diffractometer using a Cu K irradiation source (=1.54056 Å), and all the samples were scanned between 10° and 90°. Scanning electron microscopy (SEM) were obtained by Hitachi S2400 to observe the morphologies of the samples. Transmission electron microscopy (TEM), high resolution transmission electron microscopy (HRTEM), selected area electron diffraction (SAED) were acquired on a FEI Talos f200s to characterize the microstructures of the samples. X-ray photoelectron spectroscopy (XPS) measurement was enforced on a Thermo Scientific ESCALAB 250 instrument with Al Ka source to analyze the element composition. UV-visible (UV-vis) absorption spectra were acquired from a HITACHI U4100 spectrophotometer. Photoluminescence (PL) spectra were obtained using a Hitachi F-700 fluorescence spectrophotometer. Electrochemical impedance spectroscopy (EIS) and photocurrent response were measured by Chenhua CHI660E. Nitrogen adsorption-desorption isotherms were tested on the Quantachrone Autosorb iQ-MP-C.

2.4 *Photocatalytic measurement*

Photocatalytic hydrogen evolution experiments were performed in a 100 mL vacuum reactor (Perfect light Labsolar-III AG photocatalytic online analysis system), which was connected to a cryostat to maintain the reaction temperature at 9 °C during the characterization. The photocatalyst powder (10 mg) was uniformly dispersed in a 100 mL aqueous solution containing 0.35 M Na_2S and 0.25 M Na_2SO_3, and the system was vacuumed for 0.5 h to remove air. The reaction vessel was then illuminated with a 300 W xenon lamp (PLS-SXE 300C) with a cut-off filter (420 nm). Hydrogen production was tested every 0.5 h for 3 h using a gas chromatograph (FULI GC 9790) equipped with a thermal conductivity detector (TCD), and high purity Argon as the carrier gas. In the cycling test, 0.5 h dark conditions and gas draws were taken between every cycle and each cycle last for 4 h.

AQY refers to the utilization rate of photoquantum in photochemical reaction, which was gauged using visible light (420 nm) and calculated according to the following formula:[33]

$$\mathrm{AQY} = \frac{\text{the number of reacted electrons}}{\text{the number of incident photons}} \times 100\% = \frac{2 \times N_{H_2}}{\frac{I \times A \times T \times \lambda}{h \times c}} \times 100\%$$

In this formula, I = 15 A is the light intensity; t = 10800 s is the irradiation time; A is the irradiation area (about 38.5 cm^2); λ is the incident wavelength of the light source (nm); h = 6.626 × 10^{-34} Js is the Planck constant; c is the speed of light (3.0 × 10^8 m s^{-1}). All the source conditions of the above data are consistent with the hydrogen production performance test conditions.

2.5 *Electrochemical measurements*

The saturated calomel electrode (SCE) was used as the reference electrode, the platinum plate was used as the counter electrode, and the photocurrent was measured by an electrochemical analyzer (CHI660E) under a standard three-electrode structure. The working electrode was produced by three drops (30 μL per drop) of the photocatalyst suspension in 5% nafion solution/ethanol (20 mg mL^{-1}) on the surface of fluorine-doped tin oxide (FTO) glass, and then dried at room temperature. The photocurrent density at a bias voltage of 0.1 V was measured under irradiation with a 300 W Xe-lamp (optical switching period of 50 s) equipped with a 420 nm cut-off filter. The supporting electrolyte is 0.5 M of Na_2SO_4 solution. EIS were recorded in potentiation mode with a 10 mV sinusoidal wave with frequencies ranging from 100 kHz to 0.05 Hz.

3. Results and Discussion

3.1 *Characterization of samples*

The crystal structure of the as-prepared samples were determined by XRD analysis (Figure 2). Compared to the standard diffraction patterns of cubic phase ZnS (JCPDS card no. 05-0566) and hexagonal phase CdS (JCPDS card no. 41-1049), it can be seen that the diffraction pattern of $Zn_{0.5}Cd_{0.5}S$ exhibits multiphase characteristics.[4] After a certain amount of Cd were added into the ZnS crystal (for the $Zn_{0.5}Cd_{0.5}S$ sample), the diffraction peaks of $Zn_{0.5}Cd_{0.5}S$ showed an evident shift to the lower angle.[14] This phenomenon is attributed to the larger radius of Cd^{2+} than that of the Zn^{2+} ion. These results indicated the formation of the twinned $Zn_{0.5}Cd_{0.5}S$ solid solution.[17] All the peaks of Ni_2P-ZCS maintain nearly at the same position, indicating that the crystal structure of $Zn_{0.5}Cd_{0.5}S$ is not affected by the deposition of Ni_2P. However, the apparent peaks of ZCS move to a little higher angle, suggesting that ions of Zn^{2+} doped into CdS lattice. Notably, the characteristic diffraction peak of Ni_2P (Figure S1, Supplementary Information) is not observed in Ni_2P-ZCS composite, attributing to low content of Ni_2P in Ni_2P-ZCS composite which exceeds the sensitive of XRD characterization and fine particles of Ni_2P. Nevertheless, the presence of Ni_2P in

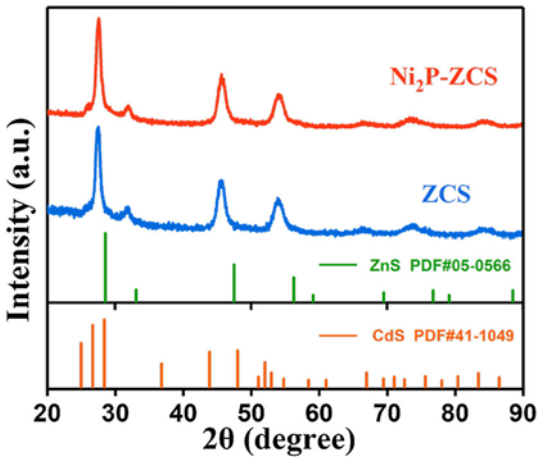

Figure 2. The XRD patterns of pure twinned ZCS and Ni_2P-ZCS nanocomposite.

Ni_2P-ZCS can be easily proved by TEM and XPS techniques, which will be discussed later.

To observe the microstructure of Ni_2P-ZCS, the prepared samples were characterized by SEM, TEM and HRTEM. SEM shows that Ni_2P-ZCS exists as an irregular granule with a size range of 30–100 nm Figure 3(a), which appears same as ZCS (Figure S2, Supplementary Information). As revealed in Figure 3(b), the twin nanocrystal structure of ZCS is confirmed by the lattice fringes of the zinc blende/wurtzite (ZB/WZ) arranged alternately and periodically arranged in twinning superlattice.[17] In addition, the black and white strips on the surface of ZCS can be observed in the TEM images (the inset of Figure 3(b)), also suggesting the existence of twinned structure of ZCS.[4] In the TEM image of Ni_2P-ZCS composite in (Figure 3(c)), some fine Ni_2P particles are found on the twinned ZCS surface with high dispersion compared with pure ZCS (Figure S3, Supplementary Information). In Figure 3(d), the identified lattice fringes of 0.32 nm correspond to the (111) lattice plane of twinned ZCS phase,[34] and the interplanar spacing of 0.22 nm is ascribed to Ni_2P (111).[35] These results indicate that Ni_2P and twinned ZCS components form a close contacted interface in the composite samples, which contributes to the efficient transfer of the charges between the components, thereby increasing the photocatalytic activity.[16] The corresponding energy-dispersive X-ray (EDX) spectra are shown in Figure 3(e–j), further demonstrating the distribution of the two substances. Obviously, the elements of Zn, Cd, S, Ni and P are coexist and distributed uniformly in the surface of Ni_2P-ZCS, further confirming that Ni_2P-ZCS composite photocatalysts are successfully prepared. In addition, the EDX results show that the molar ratio of Zn to Cd is approximately 1:1, which is consistent with the theoretical value. However, the loading amount of Ni_2P is lower than the

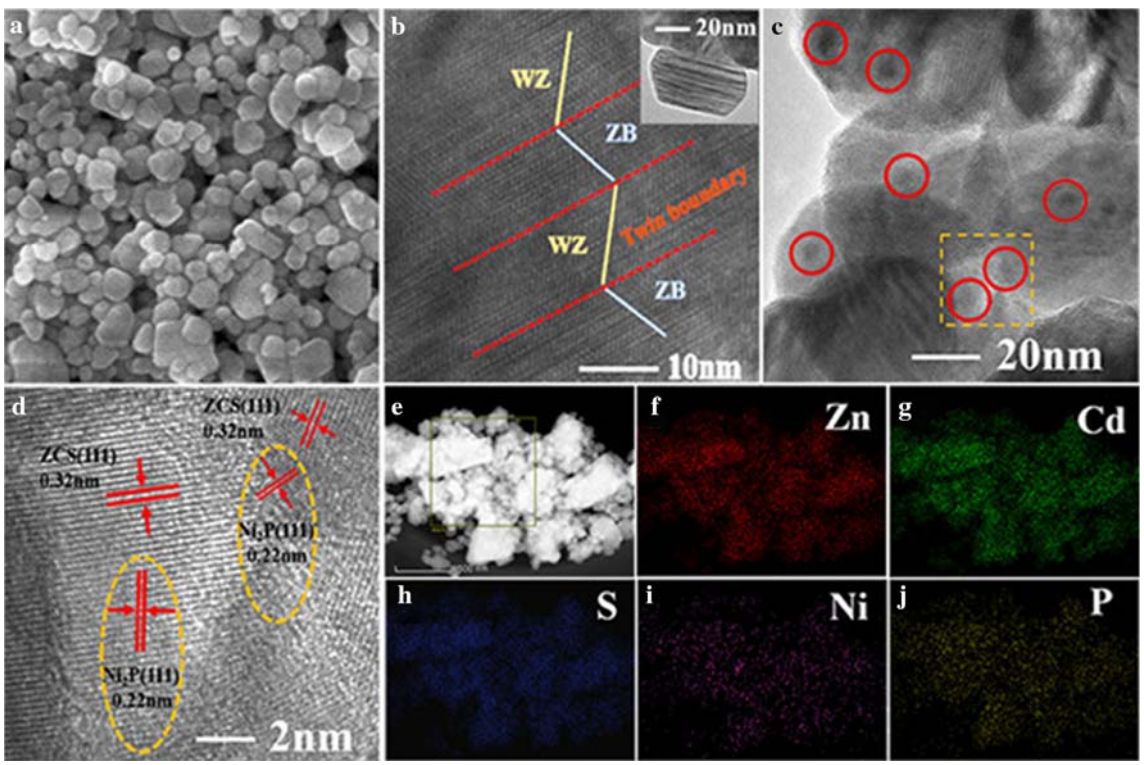

Figure 3. (a) SEM image of Ni_2P-ZCS composite; (b) Coherent twin boundaries of alternative ZB/WZ segments. (c) TEM image of Ni_2P-ZCS composite. (d) HRTEM image of Ni_2P-ZCS composite; (e-j) EDX spectra of Ni_2P-ZCS.

Table 1. EDX analysis result of Ni_2P- $Zn_{0.5}Cd_{0.5}S$.

Catalyst	Zn (wt%)	Cd (wt%)	S (wt%)	n_{Zn}:n_{Cd}:n_S
Ni_2P- $Zn_{0.5}Cd_{0.5}S$	28.39	43.57	27.46	1:1:2

theoretical value (4wt%), which is mainly because Ni^{2+} in the solution is not completely deposited on the surface of ZCS during the hydrothermal process. (Table 1, Table S1 and Figure S4, Supplementary Information).

The XPS was tested to analyze the surface chemistry and bonds of the photocatalysts. As shown in Figure 4(a), the survey spectrum provides the signal peaks of Zn, Cd, Ni, S and P elements, which is accorded with the results of EDX (Figure 3). In the high-resolution XPS spectrum of Zn 2p in Figure 4(b), two peaks at 1021.9 and 1044.9 eV correspond to Zn $2p_{3/2}$ and Zn $2p_{1/2}$, respectively, which indicates that the valence state of Zn is +2. Two peaks at 404.8 and 411.7 eV in Figure 4(c) are attributed to Cd $2p_{3/2}$ and Cd $2p_{1/2}$, which confirms the presence of Cd^{2+}. Another two peaks at 161.5 and 162.6 eV in Figure 4(d) can be assigned to S $2p_{3/2}$ and S $2p_{1/2}$, respectively.[36] The Ni 2p spectrum shows six fitted peaks (Figure 4(e)), which are related to the Ni $2p_{1/2}$ and Ni $2p_{3/2}$ energy levels. The peaks at 853.3 and 871.3 eV are ascribed to $Ni^{\delta+}$ ($0 < \delta < 2$) in Ni_2P, while two peaks at 856.3 and 876.1 eV result from the surface oxidation, and the other two peaks at 861.7 and 881.2 eV are the shake-up satellite signal related with multi-electron excitation of Ni.[15,37,38] For the P 2p spectrum in Figure 4(f), the binding energies at 129.5 and 132.9 eV are attributed to $P^{\delta-}$ of metal phosphides, following two satellite peaks at 130.6 and 133.9 eV.[38,39] These results suggest that Ni_2P is obtained and grows successfully on the surface of ZCS. Furthermore, it is noteworthy that the Zn 2p, Cd 3d and S 2p peaks of Ni_2P-ZCS composite move a little to higher binding energies compared with those of pure ZCS in Figure 4(b–d). These shifts indicate that there exists a strong interaction between ZCS and Ni_2P, which can lead to effective migration of photogenerated electrons from ZCS to Ni_2P and is expected to have superior photocatalytic performance.[35] This result is in good accordance with the above XRD, SEM, TEM, HRTEM and EDX analyses, and further demonstrate the existence of Ni, P, Cd, Zn and S for Ni_2P-ZCS. According to the XPS characterization results, we can conclude that Ni_2P was successfully deposited on the surface of $Zn_{0.5}Cd_{0.5}S$.

3.2 *Photocatalytic H_2-evolution activity and stability*

The photocatalytic H_2 evolution rates of the ZCS with different loading of Ni_2P and pure Ni_2P were carried out in visible light ($\lambda \geq 420$ nm). As presented in Figure 5, Ni_2P is inactive for photocatalytic H_2 evolution, and pure twinned ZCS has a low H_2 producing rate of 20.3 mmol h^{-1} g^{-1}. With the increase in the loading of Ni_2P, the hydrogen production rate of the product increased gradually. This can be attributed to the improved separation efficiency of photo-generated electrons at the interface between Ni_2P and ZCS and higher surface area of Ni_2P-ZCS compared to ZCS (11.03 *vs* 8.32 m^2 g^{-1}, Figure S6, Supplementary Information). The hydrogen production rate can reach the maximum value of 30.3 mmol h^{-1} g^{-1} when the Ni_2P is 4wt%. Moreover, an excess of Ni_2P may result in the marked decrease of H_2 evolution rate. These results show that Ni_2P is an effective cocatalyst for water splitting, and at the same time, excessive Ni_2P in the hybrid photocatalyst will shield the absorption of light and reduce the number of surface-active sites.

In addition to hydrogen production rate, the AQY is also a crucial parameter used to evaluate the activity for photocatalytic hydrogen production. The AQY was measured and calculated under the same conditions. The AQY value of 4wt% Ni_2P-ZCS can reach the highest value of 83.5%. Higher apparent quantum yield means higher utilization efficiency of photons in the photochemical reaction and higher photocatalytic hydrogen production rate.[38] Compared with other ZCS-based composite photocatalysts reported (Table 2), 4wt%Ni_2P-ZCS exhibits a relatively high level of H_2 evolution rate and AQY, implying its great potential application as photocatalyst. Compared with other similar systems, the excellent hydrogen production performance of Ni_2P-ZCS is mainly attributed to the following aspects: (i) ZCS has a distinctive double lattice structure (Figure 3(b)). (ii) Ni_2P is highly dispersed on the surface of ZCS with special structure (Figure 3(c)). (iii) ZCS has unique nano-twinned structure and there exists synergistic effects between the Ni_2P and the twinned ZCS (iv) The close contact between Ni_2P and twinned ZCS interface can accelerate the charge transfer.

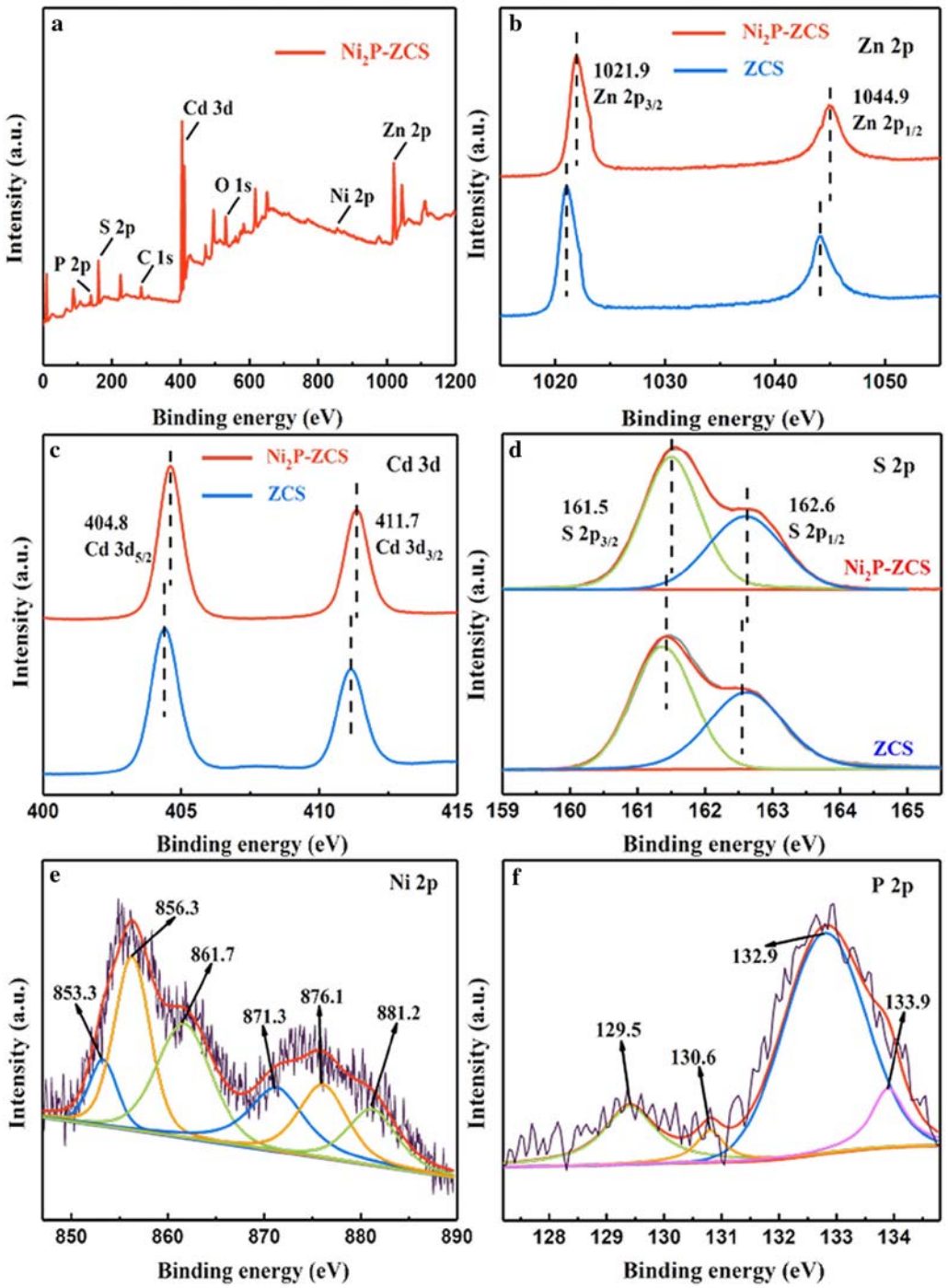

Figure 4. XPS spectra of Ni_2P-ZCS: (a) survey; (b) Zn 2p; (c) Cd 3d; (d) S 2p; (e) Ni 2p; (f) P 2p.

The stability of the photocatalysts is an important factor for their practical applications. Consequently, Ni_2P-ZCS (4wt%) was used in continuous photocatalytic process to investigate its durability (Figure 6). It is noticed that the hydrogen production rate has a slight decrease after 4-cycle continuous running, and Ni_2P-ZCS composite can maintain 90.5% of its original H_2-evolution rate. However, the activity of the pure twinned ZCS remains only 60% after four cycles. This result illustrates that 4wt%Ni_2P-ZCS composite can maintain a high stability for photocatalytic process.

3.3 *Optical and electrochemical analysis*

In order to explore the optical absorption characteristic of the as-prepared samples, the UV-vis absorption spectra were shown in Figure 7(a). It can be observed

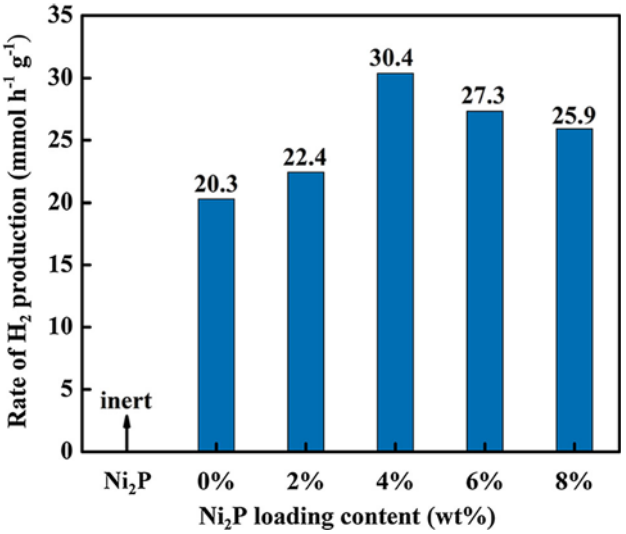

Figure 5. The rate of H_2-evolution of different samples.

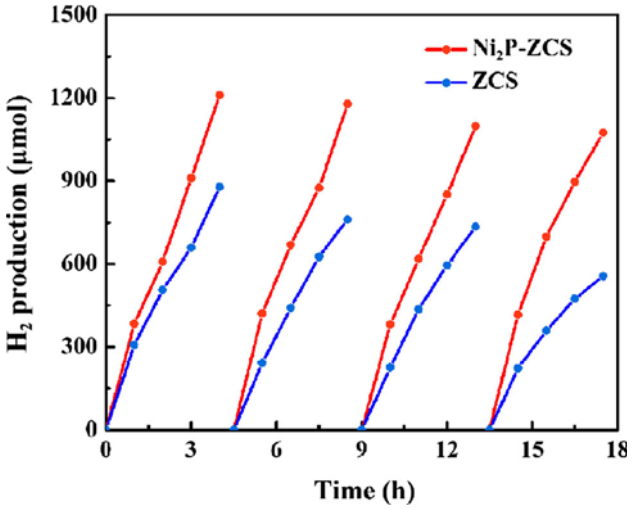

Figure 6. The cycle process of hydrogen production by photocatalysis.

that twinned ZCS and Ni_2P-ZCS have almost the same steep absorption edge in the wavelength range of 400–490 nm. The absorbance of twinned ZCS with different Ni_2P contents at the visible region ($\lambda > 490$ nm) are significantly higher than that of pure twinned ZCS, which is attributed to the absorption of Ni_2P.[35] The band gaps of the prepared samples are further calculated according to the Kubelka-Munk (KM) method through the ultraviolet pattern by the equation:[40]

$$\alpha h\nu = A(h\nu - E_g)^{1/2}$$

Here, α is the absorption coefficient; $h\nu$ is the photon energy; E_g is the direct band gap, and A is a constant. By calculation, the band gap width of the 4wt%Ni_2P-ZCS is 2.45 eV, which is smaller than ZCS (2.53 eV), leading to an enhancement in photoactivity.[36] Furthermore, the band gap width decreases with the increasing of Ni_2P loading amounts (Figure S5, Supplementary Information). The smaller band gap width means that electrons can be easily excited from valence band (VB) to conduction band (CB), which leads to higher intrinsic carrier concentration and higher conductivity. However, it should be noted that excessive Ni_2P would hinder the absorption of twinned ZCS in visible light range, which reduces the photogenic electrons and decreases the photocatalytic activity ultimately.[41]

Photoluminescence (PL) spectra of pure twinned ZCS and 4wt%Ni_2P-ZCS were obtained under an excitation wavelength of 345 nm as shown in Figure 7(b). The pure twinned ZCS has a relatively powerful emission peak at 565 nm, however, the emission intensity of Ni_2P-ZCS is significantly

Table 2. Comparative summary of photocatalytic H_2 evolution rate and AQY of different composite photocatalysts.

Photocatalyst	Catalyst dose (mg)	Visible light λ (nm)	H_2 Production ($\mu mol \cdot h^{-1} \cdot g^{-1}$)	AQY (%)	Reference
$Zn_{1-x}Cd_xS$	50	≥ 400	7420	9.6	14
NiS-MoS_2-$Zn_{0.2}Cd_{0.8}S$	20	435	41290	19	46
Pt-$Cu_{1.94}S$-$Zn_xCd_{1-x}S$	20	≥ 420	13533	26.4	21
NiS-$Zn_xCd_{1x}S$/RGO	50	≥ 420	7514	31.1	47
Ni_2P-$Zn_{0.5}Cd_{0.5}S$	100	≥ 420	9125	37.5	36
CoP NWs/ZCS	100	≥ 420	12175	4.37	48
Ni_2P-$Zn_{0.5}Cd_{0.5}S$	50	420 nm (± 5 nm)	23440	18.95	49
$Ni(OH)_2$-$Zn_{0.25}Cd_{0.75}S$	50	≥ 400	3774		45
Pt-$Zn_{0.5}Cd_{0.5}S$	30	≥ 400	5497	8.56	17
$PdP_{\sim 0.33}S_{\sim 1.67}$-$Zn_{0.5}Cd_{0.5}S$	1	≥ 420	372120	16.52	4
CoP-$Zn_{0.5}Cd_{0.5}S$	50	≥ 420	14680	73.2	34
Ni_2P-$Zn_{0.5}Cd_{0.5}S$	10	≥ 420	30373	83.5	This work

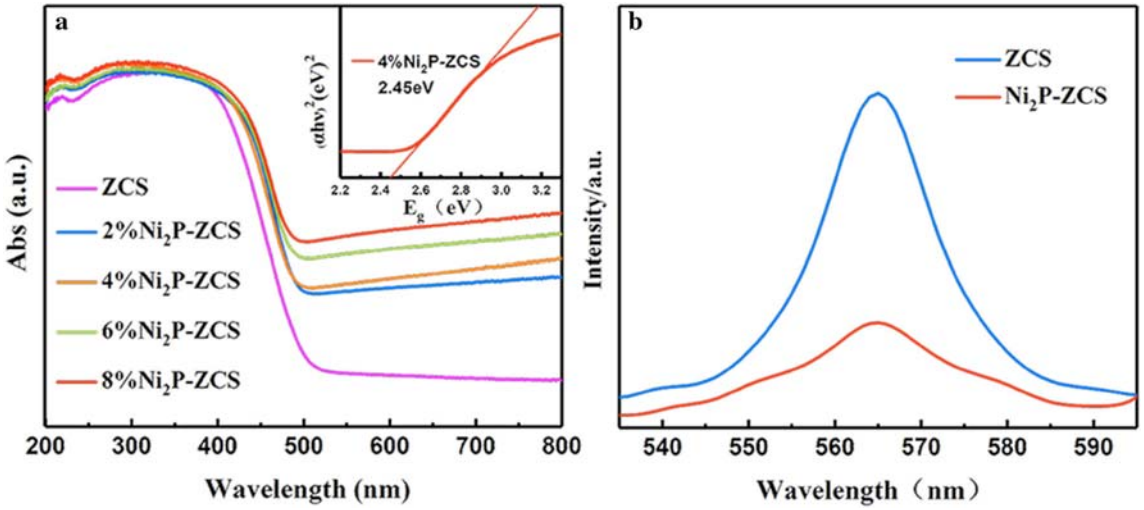

Figure 7. (a) UV–vis diffuse reflectance spectrum of pure twinned ZCS and Ni_2P-ZCS composites with different molar ratios of Ni_2P and energy band gap of 4wt%Ni_2P-ZCS; (b) photoluminescence spectra of pure twinned ZCS and 4wt%Ni_2P-ZCS.

reduced.[24] The weak emission of Ni_2P-ZCS indicates that the Ni_2P can act as charge carrier trapping center to improve separation efficiency of electron-hole pairs and decrease their recombination, thus improving the activity and stability of Ni_2P-ZCS catalyst.[42]

The transient photocurrent was used to investigate the behavior of charge separation (Figure 8(a)). Compared with response photocurrent of pure twinned ZCS, the 4wt%Ni_2P-ZCS exhibits a more rapid response rate and higher photocurrent. The photocurrent density of the Ni_2P-ZCS electrode is about three times of pure twinned ZCS. Moreover, the photocurrent response capability of pure twinned ZCS weakens gradually. The result is in good agreement with the results described above, which further proves that the Ni_2P plays an important role in improving the separation efficiency of photoelectrons at the interface of composite materials.[43]

The charge transfers resistance (RCT) of the photocatalyst was measured using EIS. Under visible-light irradiation, the pure twinned ZCS exhibits a much higher interfacial charge transfer resistance with a larger diameter than that of Ni_2P-ZCS composites (Figure 8(b)), indicating that after the introduction of Ni_2P, a faster charge transfer occurs on their interfaces. This result is consistent with the photocurrent test.[44]

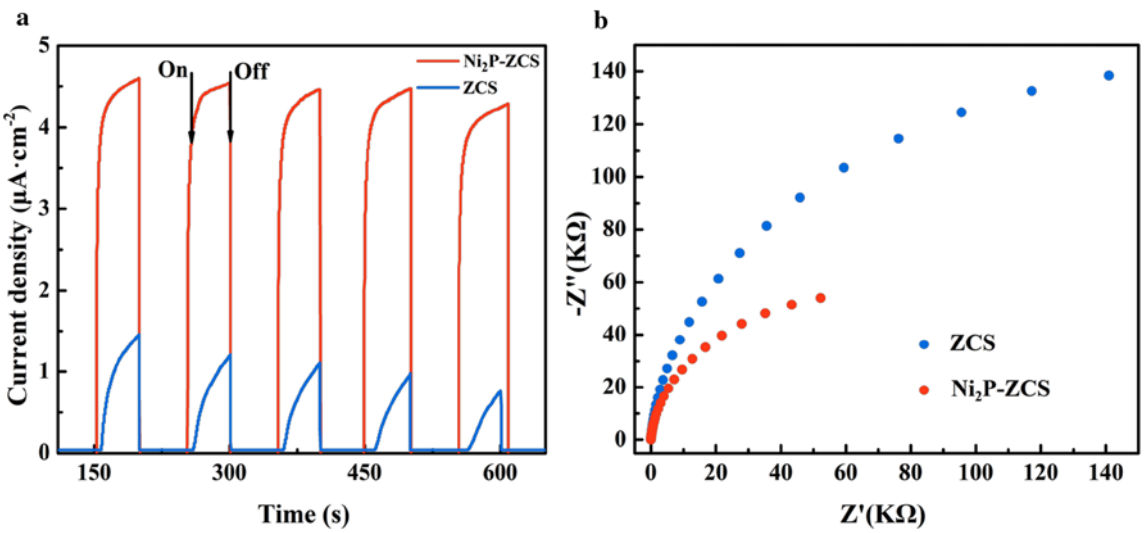

Figure 8. (a) The transient photocurrent of pure twinned ZCS and 4wt%Ni_2P-ZCS under visible light; (b) Nyquist diagram of EIS of pure twinned ZCS and 4wt%Ni_2P-ZCS.

3.4 *The mechanism of photocatalytic H_2 evolution*

On the basis of the above results, a possible photocatalytic mechanism for photocatalytic hydrogen production using Ni_2P-ZCS is proposed as depicted in Figure 9. Under the irradiation of visible light, the twinned ZCS can effectively absorb photons, and the electrons on VB are excited onto CB and the holes stayed on the VB to form photogenerated hole-electron pairs. However, without the cocatalyst, carriers may recombine rapidly, resulting in a lower rate of photocatalytic H_2 evolution of twinned ZCS. The valence band edge of ZCS is located at 2.28 eV,[4] and the conduction band edge of ZCS is calculated to be −0.25 eV, according to the formula $E_{VB} = E_{CB} + E_g$. The potential of Ni_2P is about −0.17 eV, which locates between the CB of ZCS and the potential of H^+ reduced to hydrogen molecule ($E^0_{H+/H2} = 0$). With the presence of Ni_2P catalyst, Ni_2P-ZCS exhibits high electron trapping ability due to its lower Fermi level than the pure ZCS, which makes photogenerated electron energy excite rapidly from the CB of the twinned ZCS to the surface of Ni_2P, thus effectively separating photoexcited hole-electron pairs.[34,36] Ni_2P acts as an electron collector to trap photogenerated electrons and suppress the combination of the photogenerated carriers. The electrons on Ni_2P will reduce H^+ into H_2, and the holes on the VB of ZCS are captured and consumed by the sacrificial agent in the solution. In addition, the lower H_2 adsorption energy on the surface of the Ni_2P is beneficial to the reduction of H^+. Ni_2P serves as an active reaction center in the evolution of photocatalytic H_2 and can accelerate the reaction rate.[36] Besides, the subtle atomic-level intimate contact and strong interaction between ZCS and Ni_2P provide a larger dynamic specific surface area and maximize the efficiency of electron-to-electron transmission between the two components, and thus leads to a highly efficient photocatalytic activity. Using Ni_2P-ZCS as photocatalyst under visible light ($\lambda \geq 420$ nm), the main reaction of photocatalytic H_2-evolution in an aqueous solution containing S^{2-}/SO_3^{2-} can be expressed by the following eqns. (1)–(6):

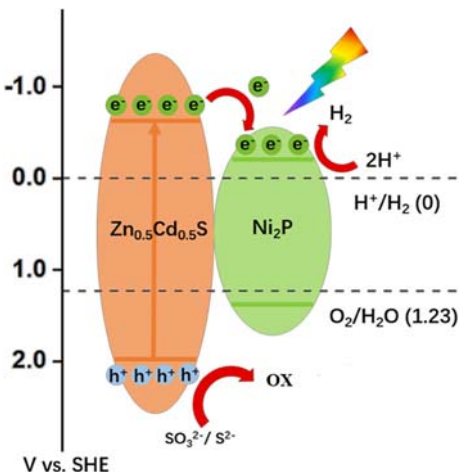

Figure 9. Schematic illustration for the charge transfer and separation in Ni_2P-ZCS system.

$$Ni_2P\text{-}ZCS \xrightarrow{h\nu} Ni_2P\ (e^-) + ZCS\ (h^+) \quad (1)$$

$$Ni_2P\ (2e^-) + 2H^+ \rightarrow Ni_2P + H_2\uparrow \quad (2)$$

$$SO_3^{2-} + H_2O + ZCS\ (h^+) \rightarrow SO_4^{2-} + 2H^+ + ZCS \quad (3)$$

$$2S^{2-} + ZCS\ (h^+) \rightarrow S_2^{2-} + ZCS \quad (4)$$

$$S_2^{2-} + SO_3^{2-} \rightarrow S_2O_3^{2-} + S^{2-} \quad (5)$$

$$SO_3^{2-} + S^{2-} + ZCS\ (h^+) \rightarrow S_2O_3^{2-} + ZCS \quad (6)$$

4. Conclusions

To sum up, we successfully synthesized high-efficiency catalysts by in-situ growth of Ni_2P on the twinned ZCS nanocrystals. The Ni_2P were scattered uniformly on the surface of twinned ZCS nanoparticles. The highest rate hydrogen evolution of 4wt%Ni_2P-ZCS can reach as high as 30473 μmol h^{-1} g^{-1} and AQY reaches 83.5% at 420 nm. Moreover, the activity retention rate could maintain 90.5% of primitive H_2-evolution rate after 4-cycle continuous catalytic process for 16 h. A possible photocatalytic mechanism was proposed to explain the enhanced evolution of H_2 in Ni_2P modified ZCS. The unique nano-twinned structure of ZCS, the close interaction between the components, and the special properties of Ni_2P can effectively isolate photogenerated electrons/holes and improve their transfer, which is instrumental to boost photocatalytic hydrogen production activity. These results indicate that Ni_2P is an effectively co-catalyst for twinned ZCS and has a potential application in the process of photocatalytic hydrogen production.

Supplementary Information (SI)

Figures S1–S6 and Table S1 are available at www.ias.ac.in/chemsci.

Acknowledgements

This work was supported by the National Natural Science Foundation of China (Grants 21706242, 21576247, and U1804140).

References

1. Liu Y, Zhang J, Guan H, Zhao Y, Yang and Zhang B 2018 Preparation of bimetallic Cu-Co nanocatalysts on poly (diallyldimethylammonium chloride) functionalized halloysite nanotubes for hydrolytic dehydrogenation of ammonia borane *Appl. Surf. Sci*. **427** 106
2. Feng J, Liu J, Cheng X, Liu J, Xu M and Zhang J 2018 Hydrothermal cation exchange enabled gradual evolution of Au@ZnS–AgAuS yolk–Shell nanocrystals and their visible light photocatalytic applications *Adv. Sci*. **5** 1700376
3. Clark R J and Felsenfeld G 1972 Electrochemcial photolysis of water at a semiconductor electrode *Nature New Biol.* **240** 226
4. Song J, Zhao H, Sun R, Li X and Sun D 2017 An efficient hydrogen evolution catalyst composed of palladium phosphorous sulphide ($PdP \sim 0.33S \sim 1.67$) and twin nanocrystal $Zn_{0.5}Cd_{0.5}S$ solid solution with both homo- and hetero-junctions *Energy Environ. Sci.* **10** 225
5. Liu M, Wang L, Lu G, Yao X and Guo L 2011 Twins in $Cd_{1-x}Zn_xS$ solid solution: Highly efficient photocatalyst for hydrogen generation from water *Energy Environ. Sci.* **4** 1372
6. Tijare S N, Bakardjieva S, Subrt J, Joshi M V, Rayalu S S, Hishita S and Labhsetwar N 2014 Synthesis and visible light photocatalytic activity of nanocrystalline $PrFeO_3$ perovskite for hydrogen generation in ethanol–water system *J. Chem. Sci.* **126** 517
7. Lou Y, Zhang Y, Cheng L, Chen J and Zhao Y 2018 A stable plasmonic $Cu@Cu_2O/ZnO$ heterojunction for enhanced photocatalytic hydrogen generation *ChemSusChem.* **11** 1505
8. Iwashina K, Iwase A, Ng Y H, Amal R and Kudo A 2015 Z-schematic water splitting into H_2 and O_2 using metal sulfide as a hydrogen-evolving photocatalyst and reduced graphene oxide as a solid-state electron mediator *J. Am. Chem. Soc.* **137** 604
9. Liang Y-H, Liao M-W, Mishra M and Perng T-P 2019 Fabrication of Ta_3N_5ZnO direct Z-scheme photocatalyst for hydrogen generation *Int. J. Hydrogen Energy* **44** 19162
10. Reshak A H 2018 Active photocatalytic water splitting solar-to-hydrogen energy conversion: Chalcogenide photocatalyst Ba_2ZnSe_3 under visible irradiation *Appl. Catal. B Environ.* **221** 17
11. Xiang Z, Nan J, Deng J, Shi Y, Zhao Y, Zhang B and Xiang X 2019 Uniform CdS-decorated carbon microsheets with enhanced photocatalytic hydrogen evolution under visible-light irradiation *J. Alloys Compd.* **770** 886
12. Song K, Zhu R, Tian F, Cao G and Ouyang F 2015 Journal of solid state chemistry effects of indium contents on photocatalytic performance of $ZnIn_2S_4$ for hydrogen evolution under visible light *J. Solid State Chem.* **232** 138
13. Ma D, Shi J-W, Zou Y, Fan Z, Shi J, Cheng L, Sun D, Wang Z and Niu C 2018 Multiple carrier-transfer pathways in a flower-like $In_2S_3/CdIn_2S_4/In_2O_3$ ternary heterostructure for enhanced photocatalytic hydrogen production *Nanoscale* **10** 7860
14. Li Q, Meng H, Zhou P, Zheng Y, Wang J, Yu J and Gong J 2013 $Zn_{1-x}Cd_xS$ solid solutions with controlled bandgap and enhanced visible-Light photocatalytic H_2-production activity *ACS Catal.* **3** 882
15. Zhao H, Liu H, Sun R, Chen Y and Li X 2018 A $Zn_{0.5}Cd_{0.5}S$ photocatalyst modified by 2D black phosphorus for efficient hydrogen evolution from water *ChemCatChem.***10** 4395
16. Li X-l, Wang X-j, Zhu J-Y, Li Y-P, Zhao J and Li F-T 2018 Fabrication of two-dimensional $Ni_2P/ZnIn_2S_4$ heterostructures for enhanced photocatalytic hydrogen evolution *Chem. Eng. J.* **353** 15
17. Ng B-J, Putri L K, Kong X Y, Shak K P Y, Pasbakhsh P, Chai S-P and Mohamed A R 2018 Sub-2nm Pt-decorated $Zn_{0.5}Cd_{0.5}S$ nanocrystals with twin-induced homojunctions for efficient visible-light-driven photocatalytic H_2 evolution *Appl. Catal. B Environ.* **224** 360
18. Abdel M and Al-johani H 2017 Enhancement of visible light irradiation photocatalytic activity of $SrTiO_3$ nanoparticles by Pt doping for oxidation of cyclohexane *J. Chem. Sci.* **129** 1687
19. Manbeck G F, Fujita E and Brewer K J 2017 Tetra and Heptametallic Ru(II), Rh(III) Supramolecular Hydrogen Production Photocatalysts *J. Am. Chem. Soc.* **139** 7843
20. Wang C-C, Chang J-W and Lu S-Y 2017 p-Cu_2S/n-$Zn_xCd_{1-x}S$ nanocrystals dispersed in a 3D porous graphene nanostructure: an excellent photocatalyst for hydrogen generation through sunlight driven water splitting *Cat. Sci. Technol.* **7** 1305
21. Chen Y, Zhao S, Wang X, Peng Q, Lin R, Wang Y, Shen R, Cao X, Zhang L, Zhou G, Li J, Xia A and Li Y 2016 Synergetic integration of $Cu_{1.94}S$-$Zn_xCd_{1-x}S$ heteronanorods for enhanced visible-light-driven photocatalytic hydrogen production *J. Am. Chem. Soc.* **138** 4286
22. Liu M, Chen Y, Su J, Shi J, Wang X and Guo L 2016 Photocatalytic hydrogen production using twinned nanocrystals and an unanchored NiS_x co-catalyst *Nat. Energy* **1** 16151
23. Yin M, Zhang W, Qiao F, Sun J, Fan Y and Li Z 2019 Hydrothermal synthesis of MoS_2-NiS/CdS with enhanced photocatalytic hydrogen production activity and stability *J. Solid State Chem.* **270** 531
24. Zheng M, Ding Y, Yu L, Du X and Zhao Y 2017 In situ grown pristine cobalt sulfide as bifunctional photocatalyst for hydrogen and oxygen evolution *Adv. Funct. Mater.* **27** 1605846
25. Wang P, Lu Y, Wang X and Yu H 2017 Co-modification of amorphous-Ti(IV) hole cocatalyst and $Ni(OH)_2$ electron cocatalyst for enhanced photocatalytic H_2-production performance of TiO_2 *Appl. Surf. Sci.* **391** 259
26. Zhou X, Jin J, Zhu X, Huang J, Yu J, Wong W-Y and Wong W-K 2016 New $Co(OH)_2$/CdS nanowires for efficient visible light photocatalytic hydrogen production *J. Mater. Chem. A* **4** 5282

27. Yue X, Yi S, Wang R, Zhang Z and Qiu S 2016 A novel and highly efficient earth-abundant Cu_3P with TiO_2 "P-N" heterojunction nanophotocatalyst for hydrogen evolution from water *Nanoscale* **8** 17516
28. Zeng D, Ong W-J, Chen Y, Tee S Y, Chua C S, Peng D-L and Han M-Y, 2018 Co_2P nanorods as an efficient cocatalyst decorated porous g-C_3N_4 nanosheets for photocatalytic hydrogen production under visible light irradiation *Part. Part. Syst. Char.* **35** 1700251
29. Qiu B, Zhu Q, Xing M and Zhang J 2017 A robust and efficient catalyst of $Cd_xZn_{1-x}Se$ motivated by CoP for photocatalytic hydrogen evolution under sunlight irradiation *Chem. Commun.* **53** 897
30. Sun Z, Zheng H, Li J and Du P 2015 Extraordinarily efficient photocatalytic hydrogen evolution in water using semiconductor nanorods integrated with crystalline Ni_2P cocatalysts *Energy Environ Sci.* **8** 2668
31. Wu T, Wang P, Ao Y and Wang C 2018 Enhanced visible light activated hydrogen evolution activity over cadmium sulfide nanorods by the synergetic effect of a thin carbon layer and noble metal-free nickel phosphide cocatalyst *J. Colloid Interface Sci.* **525** 107
32. Qin Z, Xue F, Chen Y, Shen S and Guo L 2017 Spatial charge separation of one-dimensional Ni_2P-$Cd_{09}Zn_{01}S$/g-C_3N_4 heterostructure for high-quantum-yield photocatalytic hydrogen production *Appl. Catal. B Environ.* **217** 551
33. Lin H, Li Y, Li H and Wang X 2017 Multi-node CdS hetero-nanowires grown with defect-rich oxygen-doped MoS_2 ultrathin nanosheets for efficient visible-light photocatalytic H_2 evolution *Nano Res.* **10** 1377
34. Dai D, Xu H, Ge L, Han C, Gao Y, Li S and Lu Y 2017 In-situ synthesis of CoP co-catalyst decorated Zn_{05}-$Cd_{05}S$ photocatalysts with enhanced photocatalytic hydrogen production activity under visible light irradiation *Appl. Catal. B Environ.* **217** 429
35. Peng S, Yang Y, Tan J, Gan C and Li Y 2018 In situ loading of Ni_2P on $Cd_{05}Zn_{05}S$ with red phosphorus for enhanced visible light photocatalytic H_2 evolution *Appl. Surf. Sci.* **447** 822
36. Shao Z, He Y, Zeng T, Yang Y, Pu X, Ge B and Dou J 2018 Highly efficient photocatalytic H_2 evolution using the Ni_2P-$Zn_{05}Cd_{05}S$ photocatalyst under visible light irradiation *J. Alloys Compd.* **769** 889
37. Zhou D, Xue L-P and Wang N 2019 Robustly immobilized Ni_2P nanoparticles in porous carbon networks promotes high-performance sodium-ion storage *J. Alloys Compd.* **776** 912
38. Calvinho K, Laursen A and Yap K 2018 Selective CO_2 reduction to C_3 and C_4 oxyhydrocarbons on nickel phosphides at overpotentials as low as 10 mV *Energy Environ. Sci.* **11** 2550
39. Wang Z, Jin Z, Yuan H, Wang G and Ma B 2018 Orderly-designed Ni_2P nanoparticles on g-C_3N_4 and UiO-66 for efficient solar water splitting *J. Colloid Interf. Sci.* **532** 287
40. Li Y, Ouyang S, Xu H, Wang X, Bi Y, Zhang Y and Ye J 2016 Constructing solid-gas-interfacial fenton reaction over alkalinized-C_3N_4 photocatalyst to achieve apparent quantum yield of 49% at 420 nm *J. Am. Chem. Soc.* **138** 13289
41. Lu Y, Shang H, Guan H, Zhao Y and Zhang B 2015 Enhanced visible-light photocatalytic activity of $BiVO_4$ microstructures via annealing process *Superlattic Microst.* **88** 591
42. Ran J, Gao G, Li F T, Ma T Y, Du A and Qiao S-Z 2017 Ti_3C_2 MXene co-catalyst on metal sulfide photo-absorbers for enhanced visible-light photocatalytic hydrogen production *Nat. Commun.* **8** 13907
43. Zhang J, Qi L, Ran J, Yu J and Qiao S-Z 2014 Ternary NiS/$Zn_xCd_{1-x}S$/Reduced Graphene Oxide Nanocomposites for Enhanced Solar Photocatalytic H_2-Production Activity *Adv. Energy Mater.* **4** 1301925
44. Lu Z, Li C, Han J, Wang L, Wang S, Ni L and Wang Y 2018 Construction 0D/2D heterojunction by highly dispersed Ni_2P QDs loaded on the ultrathin g-C_3N_4 surface towards superhigh photocatalytic and photoelectric performance *Appl. Catal. B Environ.* **237** 919
45. Xu Y, Gong Y, Ren H, Liu W, Li C, Liu X and Niu L 2018 Insight into enhanced photocatalytic H_2 production by $Ni(OH)_2$-decorated $Zn_xCd_{1-x}S$ nanocomposite photocatalysts *J. Alloys Compd.* **735** 2551
46. An C, Feng J, Liu J, Wei G, Du J and Wang H 2017 NiS nanoparticle decorated MoS_2 nanosheets as efficient promoters for enhanced solar H_2 evolution over Zn_x-$Cd_{1-x}S$ nanorods as efficient promoters for enhanced solar H_2 *Inorg. Chem. Front.* **4** 1042
47. Zhang J, Qi L, Ran J, Yu J and Qiao S-Z 2014 Ternary NiS/$Zn_xCd_{1-x}S$/reduced graphene oxide nanocomposites for enhanced solar photocatalytic H_2-production activity *Adv. Energy Mater.* **4** 1301925
48. Wang P, Zhan S, Wang H, Xia Y, Hou Q, Zhou Q, Li Y and Kumar R R 2018 Cobalt phosphide nanowires as efficient co-catalyst for photocatalytic hydrogen evolution over $Zn_{05}Cd_{05}S$ *Appl. Catal. B Environ.* **230** 210
49. Dai D, Wang L, Xiao N, Li S, Xu H, Liu S, Xu B, Lv D, Gao Y, Song W, Ge L and Liu J 2018 In-situ synthesis of Ni_2P co-catalyst decorated $Zn_{05}Cd_{05}S$ nanorods for high-quantum-yield photocatalytic hydrogen production under visible light irradiation *Appl. Catal. B Environ.* **233** 194